Scientific Research Publishing

Materials Sciences and Applications, 2023, 14, 397-406
https://www.scirp.org/journal/msa
ISSN Online: 2153-1188
ISSN Print: 2153-117X

Depth Profile Study of Electroless Deposited Sb_2S_3 Thin Films Using XPS for Photovoltaic Applications

Towhid Adnan Chowdhury

Department of Electrical & Electronic Engineering, Ahsanullah University of Science & Technology, Dhaka, Bangladesh
Email: towhid6789@yahoo.com

How to cite this paper: Chowdhury, T.A. (2023) Depth Profile Study of Electroless Deposited Sb_2S_3 Thin Films Using XPS for Photovoltaic Applications. *Materials Sciences and Applications*, **14**, 397-406.
https://doi.org/10.4236/msa.2023.147025

Received: June 1, 2023
Accepted: July 16, 2023
Published: July 19, 2023

Abstract

Sb_2S_3 has gained tremendous research recently for thin film solar cell absorber material because of their easy synthesis, unique electrical and optical properties. The stoichiometry and composition of electroless Sb_2S_3 thin films were analyzed using XPS depth profile studies. The surface layers were found nearly stoichiometric. On the other hand, the inner layer was rich in antimony composition making it more conductive electrically.

Keywords

Sb_2S_3, Depth Profiling, X-Ray Photoelectron Spectroscopy, Thin Film, Electroless

1. Introduction

Photovoltaic technologies implement a long-term, clean and cost-effective solution to fulfill increasing demand of energy by converting solar energy into electricity [1] [2] [3] [4] [5]. It is regrettable that most of this energy is not being used using solar cells because of the environmental pollution and high cost involved in solar cell fabrication [6]. Therefore, the main objective of solar energy research has become to look for stable, efficient, low-cost and environmentally friendly solar cell materials [7] [8]. In this regard, metal chalcogenide solar cells, such as CdTe [9], Cu(In, Ga)Se_2 [10], $Cu_2ZnSn(S, Se)_4$ (CZTSSe) [11], Sb_2S_3 [12] and Sb_2Se_3 [13] have played important roles in solar energy usages. Due to high absorption coefficiency ($\alpha > 10^4$ cm^{-1}), elemental content which is environmentally friendly and suitable band gap (1.70 - 1.90 eV) Sb_2S_3 is a promising material among them [14] [15] [16] [17].

Antimony trisulfide (Sb_2S_3) has gained particular research attention owing to

its high thermoelectric power, suitable valence band position and good photovoltaic properties [18] [19] [20]. This material has been applied in various fields such as thermoelectric cooling devices, optoelectronic devices, switching devices, microwave, visible light-responsive photocatalysis, optical data storage devices and photovoltaic structures [21]-[34]. It is essential to have an idea of stoichiometry of surface and bulk of Sb_2S_3 film as it has a profound impact on cell performance. In the present work, Sb_2S_3 thin films were first synthesized by electroless deposition. Then stoichiometry of Sb_2S_3 thin films was investigated using X-ray photoelectron spectroscopy (XPS) depth profiling.

2. Experimental Details

All the glassware in the experiment has been cleaned by first washing and scrubbing with alconox, followed by a 20 min. sonication in acetone, methanol, and then washed by DI water and isopropanol. Afterwards, the glassware was dried using N_2 gas. An aqueous solution of 650 mg $SbCl_3$, 25 ml $Na_2S_2O_3$, 2.5 ml acetone and 72.5 ml water have been used for precursor solution electroless deposition. The precursor solution was continuously stirred for the duration of the experiment to assure a good dispersion of precursor materials in the solution. Substrate temperature was controlled by a hot plate with which a thermocouple was attached. The substrate temperature was maintained within ±1˚C of 10˚C for 4 hours.

Composition of the Sb_2S_3 thin film was studied using XPS. The XPS spectra were obtained by using monochromatic Al Kα radiation (1486.6 eV). through a Kratos AXIS Ultra DLD XPS system at a base pressure of 5×10^{-10} Torr, equipped with an electronic neutralization gun to eliminate the charge effect on the sample surface. The sample was firstly pressed to a 1 × 13 mm disc and fixed to the sample-holder, then it was degassed in the load lock chamber overnight. After that, it was removed to the test chamber for XPS study. All binding energy values were calibrated by using the value of contaminant carbon (C 1s 284.6 eV) as a reference. The sample was then ion sputtered with Ar^+ at 4000 eV and 15 mA for 1 min and 10 min. The raster area is approximately 6 mm × 6 mm, and the estimated erosion rate for depth profiling study during sputter is 4 nm/min.

XPSPeak software version 4.1 was used to fit all the spectra. The spectra were doconvoluted using a mixture of Lorentzian-Gaussian type peaks and Shirley background was applied in all cases.

3. Results and Discussion

The chemical purity and the composition of Sb_2S_3 thin films were investigated by XPS analysis. The typical XPS survey spectrum of Sb_2S_3 is showed in **Figure 1(a)**. The peaks arising from Sb 4d, 3d, 3p, 3s, Sb Auger, Na 1s, Na Auger, O 2s, O Auger, C 1s, C Auger, S 2p and 2s are clearly seen in the spectrum. No other impurities are observed in the spectrum. Carbon contamination is impossible to avoid in almost all the preparations. All other peaks that arise due to energy loss

features on the major peaks are weak and broad. The Sb 3d intensity is very large compared to the Sb 4d intensity, and that is why we have studied just Sb 3d spectra of Sb compounds high resolution spectra of Sb 3d core level and S 2p core level are shown in the **Figure 1(b)** and **Figure 1(c)** respectively. The two peaks at 530.2 eV and 539.5 eV can be assigned to the binding energy of Sb $3d_{5/2}$ and $3d_{3/2}$ respectively. The separation of Sb 3d doublet is by 9.3 eV. These binding energy values of Sb 3d are characteristic of antimony in the metal sulfides (Sb_2S_3) [35]. The presence of Oxygen 1s in the surface may be due to our deposition method. It confirmed that Sb_2S_3 could be easily oxidized. The Na Auger peak that is present on the surface that is found in the high resolution spectra of Sb 3d core level is due to precursor solution used for the deposition. The peak of S centered at binding energy of 161.3 eV (**Figure 1(c)**) corresponds to S in metal sulfides (Sb_2S_3) [36].

The XPS survey spectrum of Sb_2S_3 thin film after 1 min. Ar^+ ion sputtering is showed in **Figure 2(a)**. The peaks arising from Sb 4d, 3d, 3p, 3s, Sb Auger, Na 1s, Na Auger, O 2s, O Auger, C 1s, C Auger, S 2p and 2s are clearly seen in the spectrum. Oxygen and Carbon contaminations on the surface were reduced significantly after 1 min. Ar^+ ion sputtering. High resolution spectra of Sb 3d core level and S 2p core level are shown in the **Figure 2(b)** and **Figure 2(c)** respectively. The two peaks at 530.1 eV and 539.4 eV can be assigned to the binding energy of Sb $3d_{5/2}$ and $3d_{3/2}$. The separation of Sb 3d doublet is by 9.3 eV. These binding energy values of Sb 3d are characteristic of antimony in the metal sulfides (Sb_2S_3) [35]. A chemical shift of 0.1 eV was observed in Sb $3d_{5/2}$ after 1 min. Ar^+ ion sputtering. The Oxygen 1s and Na Auger peak that is found in the high resolution spectra of Sb 3d core level is reduced compared with as-deposited Sb_2S_3 film. After 1 min of Ar^+ ion sputtering, sulfur can be detected in two states, one with binding energy at 162.0 eV and one at 161.1 eV. These binding energy values of S 2p are characteristic of sulfur in the metal sulfides (Sb_2S_3) [35]. The binding energy differences indicate the small changes of the chemical environment of the Sb and S atoms [37].

The XPS survey spectrum of Sb_2S_3 thin film after 10 min. Ar^+ ion sputtering is showed in **Figure 3(a)**. The peaks arising from Sb 4d, 3d, 3p, 3s, Sb Auger, Na 1s, Na Auger, O 2s, O Auger, C 1s, C Auger, S 2p and 2s are clearly seen in the spectrum. Oxygen and Carbon contaminations on the surface were reduced significantly after 10 min. Ar^+ ion sputtering. High resolution spectra of Sb 3d core level and S 2p core level are shown in the **Figure 3(b)** and **Figure 3(c)** respectively. After 10 min of Ar^+ ion sputtering, we can observe that antimony is in two states, one with binding energy at 530.1 eV corresponding to Sb_2S_3 and one at 528.1 eV corresponding to Sb in metallic state [35]. The two peaks at 530.1 eV and 539.4 eV can be assigned to the binding energy of Sb $3d_{5/2}$ and $3d_{3/2}$. The separation of Sb 3d doublet is by 9.3 eV. A chemical shift of 0.1 eV was observed in Sb $3d_{5/2}$ after 10 min. Ar^+ ion sputtering relative to as-deposited film. The Oxygen 1s and Na Auger peak that is found in the high resolution spectra of Sb 3d

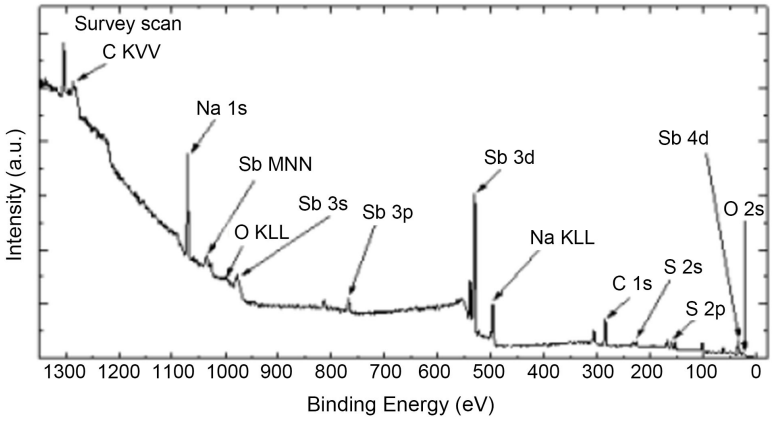

(a)

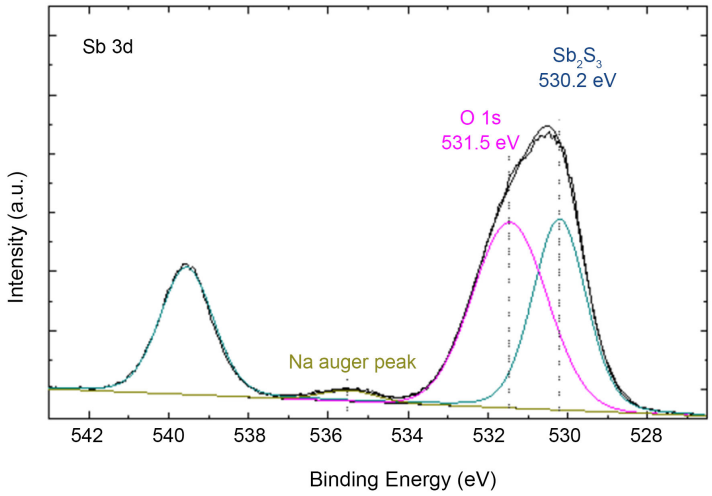

(b)

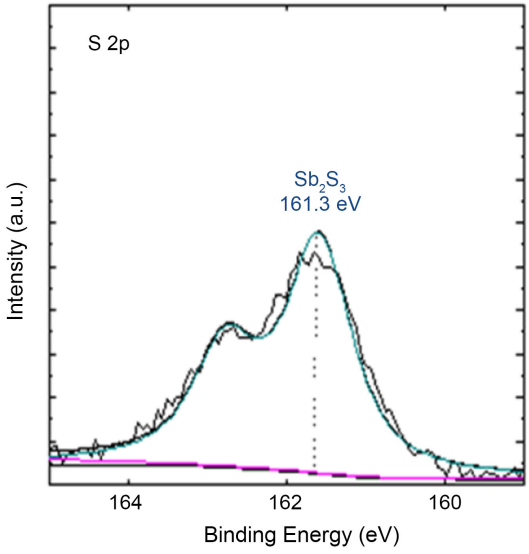

(c)

Figure 1. (a) XPS survey spectrum of as-deposited Sb_2S_3 film; (b) high resolution XPS spectra of the Sb 3d core level of as-deposited Sb_2S_3 film; (c) high resolution XPS spectra of the S 2p core level of as-deposited Sb_2S_3 film.

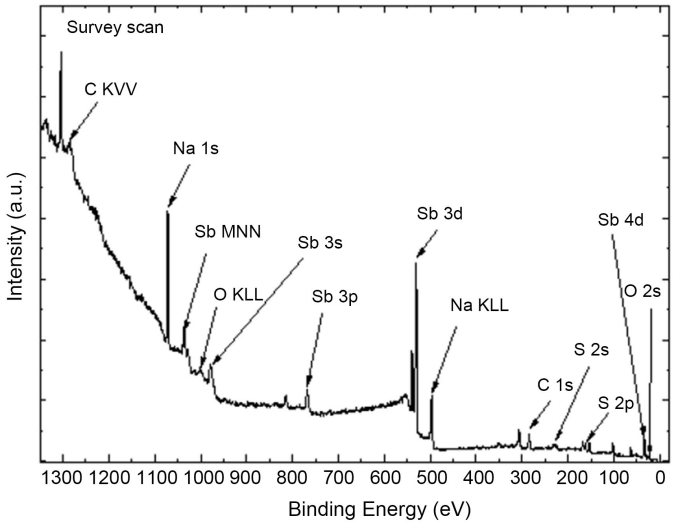

(a)

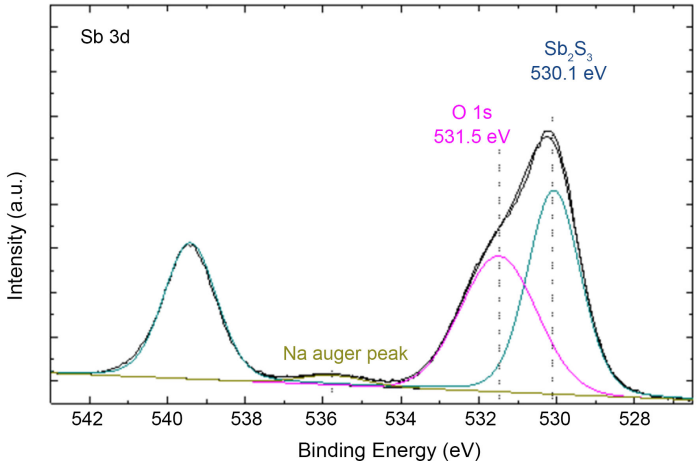

(b)

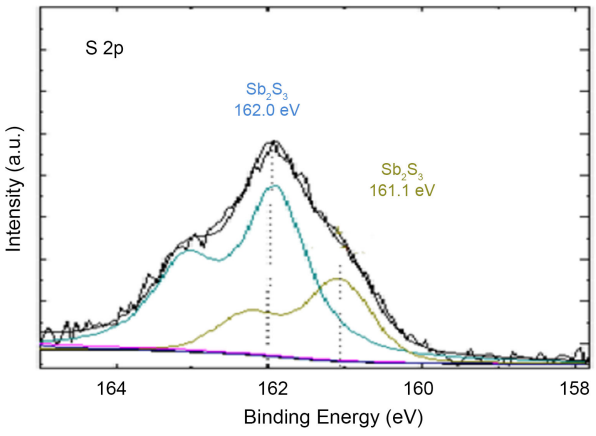

(c)

Figure 2. (a) XPS survey spectrum of Sb_2S_3 film after 1 min. Ar^+ ion sputtering; (b) high resolution XPS spectra of the Sb 3d core level of Sb_2S_3 film after 1 min. Ar^+ ion sputtering; (c) high resolution XPS spectra of the S 2p core level of Sb_2S_3 film after 1 min. Ar^+ ion sputtering.

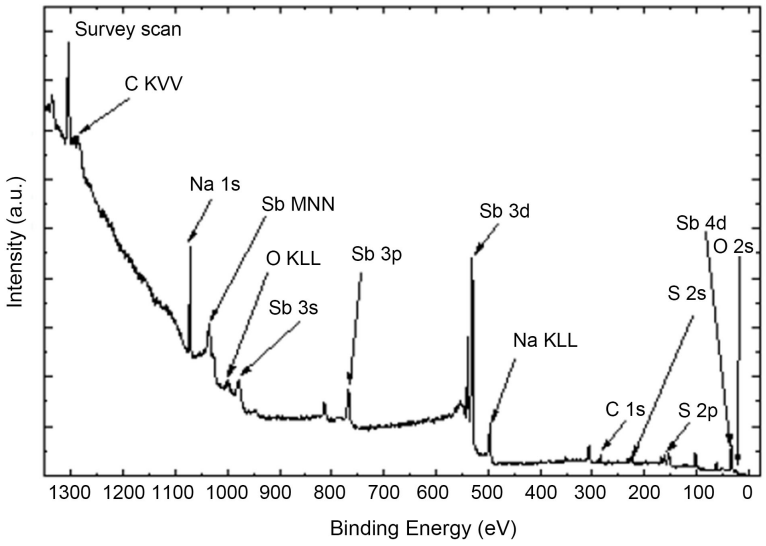

(a)

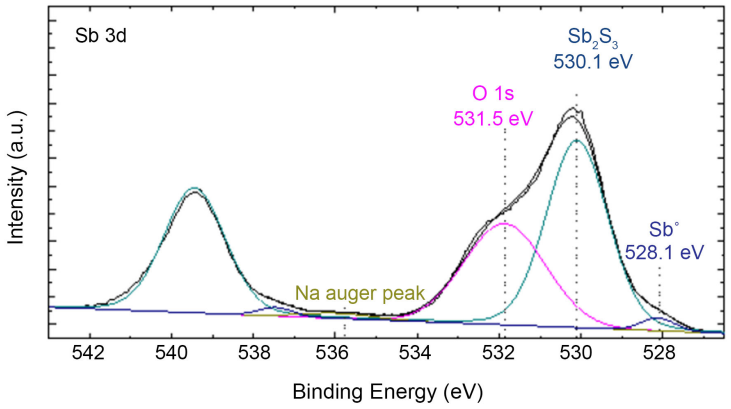

(b)

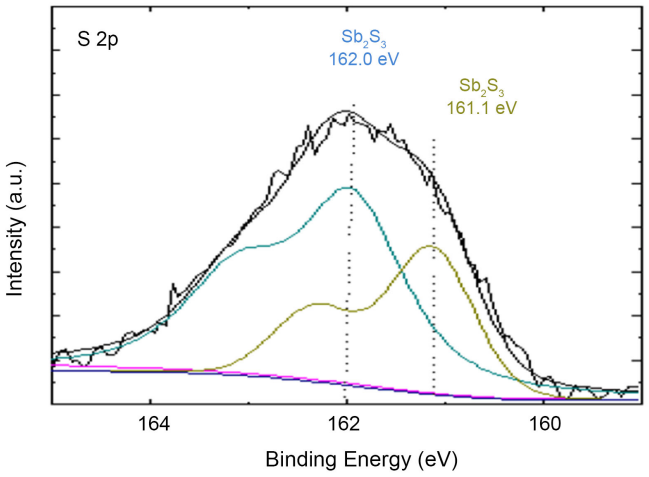

(c)

Figure 3. (a) XPS survey spectrum of Sb_2S_3 film after 10 min. Ar^+ ion sputtering; (b) high resolution XPS spectra of the Sb 3d core level of Sb_2S_3 film after 10 min. Ar^+ ion sputtering; (c) high resolution XPS spectra of the S 2p core level of Sb_2S_3 film after 10 min. Ar^+ ion sputtering.

core level is reduced significantly compared with as-deposited Sb_2S_3 film. Sulfur can be detected in two states as we found with 1 min of Ar^+ ion sputtering, one with binding energy at 162.0 eV and one at 161.1 eV. These binding energy values of S 2p are characteristic of sulfur in the metal sulfides (Sb_2S_3) [35]. The binding energy differences indicate the small changes of the chemical environment of the Sb and S atoms [37].

4. Conclusion

The Sb_2S_3 is sensitive to air. The oxide phase of Sb_2S_3 affects the cell performance. It is important to analyze the purity of the as-deposited film because oxygen impurity may create recombination centers resulting in deterioration of the cell performance. To this point of view, we examined the purity of Sb_2S_3 using powerful depth-profiling X-ray photoelectron spectroscopy (XPS). XPS depth profile analysis in this report reveals that composition of Sb_2S_3 thin films close to surface is almost stoichiometric. As sputter time is increased, the peak intensity of O(1s) becomes lower because of lower oxygen content at deeper surface. The Sb 3d core level binding energy is decreased by 0.1 eV during Ar^+ ion sputtering. Sulfur can be detected in two states as we found during Ar^+ ion sputtering. The binding energy differences indicate the small changes of the chemical environment of the Sb and S atoms. After 10 min. of Ar^+ ion sputtering, we can observe that antimony is in two states. One as antimony sulfide (Sb_2S_3) and other as Sb in metallic state.

Acknowledgements

The work was supported by the Advanced Support Program for Innovative Research Excellence-(ASPIRE-I), grant number 15530-E404 and Support to Promote Advancement of Research and Creativity (SPARC), grant number 15530-E413 of the University of South Carolina, Columbia, USA.

Conflicts of Interest

The author declares no conflicts of interest regarding the publication of this paper.

References

[1] Wang, X.M., Tang, R.F., Wu, C.Y., Zhu, C.F. and Chen, T. (2018) Development of Antimony Sulfide—Selenide $Sb_2(S, Se)_3$-Based Solar Cells. *Journal of Energy Chemistry*, **27**, 713-721. https://doi.org/10.1016/j.jechem.2017.09.031

[2] Hossain, M.K., Raihan, G.A., Akbar, M.A., Rubel, M.H.K., Ahmed, M.H., Khan, M.I., Hossain, S., Sen, S.K., Jalal, M.I.E. and El-Denglawey, A. (2022) Current Applications and Future Potential of Rare Earth Oxides in Sustainable Nuclear, rAdiation, and Energy Devices: A Review. *ACS Applied Electronic Materials*, **4**, 3327-3353. https://doi.org/10.1021/acsaelm.2c00069

[3] Green, M.A. (2019) How Did Solar Cells Get so Cheap? *Joule*, **3**, 631-633. https://doi.org/10.1016/j.joule.2019.02.010

[4] Hossain, M.K., Pervez, M.F., Tayyaba, S., Uddin, M.J., Mortuza, A.A., Mia, M.N.H., Manir, M.S., Karim, M.R. and Khan, M.A. (2017) Efficiency Enhancement of Natural Dye Sensitized Solar Cell by Optimizing Electrode Fabrication Parameters. *Materials Science*, **35**, 816-823. https://doi.org/10.1515/msp-2017-0086

[5] Hossain, M.K., Pervez, M.F., Mia, M.N.H., Mortuza, A.A., Rahaman, M.S., Karim, M.R., Islam, J.M.M., Ahmed, F. and Khan, M.A. (2017) Effect of Dye Extracting Solvents and Sensitization Time on Photovoltaic Performance of Natural Dye Sensitized Solar Cells. *Results in Physics*, **7**, 1516-1523. https://doi.org/10.1016/j.rinp.2017.04.011

[6] Tong, J., Song, Z., Kim, D.H., Chen, X., Chen, C., Palmstrom, A.F., Ndione, P.F., Reese, M.O., Dunfield, S.P., Reid, O.G., Liu, J., Zhang, F., Harvey, S.P., Li, Z., Christensen, S.T., Teeter, G., Zhao, D., Al-Jassim, M.M., Van Hest, M.F.A.M., Beard, M.C., Shaheen, S.E., Berry, J.J., Yan, Y. and Zhu, K. (2019) Carrier Lifetimes of >1 μs in Sn-Pb Perovskites Enable Efficient All-Perovskite Tandem Solar Cells. *Science*, **364**, 475-479. https://doi.org/10.1126/science.aav7911

[7] Zhang, H., Xiao, J., Shi, J., Su, H., Luo, Y., Li, D., Wu, H., Cheng, Y.B. and Meng, O. (2018) Self-Adhesive Macroporous Carbon Electrodes for Efficient and Stable Perovskite Solar Cells. *Advanced Functional Materials*, **28**, Article ID: 1802985. https://doi.org/10.1002/adfm.201802985

[8] Wu, W.Q., Wang, Q., Fang, Y., Shao, Y., Tang, S., Deng, Y., Lu, H., Liu, Y., Li, T., Yang, Z., Gruverman, A. and Huang, J. (2018) Molecular Doping Enabled Scalable Blading of Efficient Hole-Transport-Layer-Free Perovskite Solar Cells. *Nature Communications*, **9**, Article No. 1625. https://doi.org/10.1038/s41467-018-04028-8

[9] Burst, J.M., Duenow, J.N., Albin, D.S., Colegrove, E., Reese, M.O., Aguiar, J.A., Jiang, C.S., Patel, M.K., Al-Jassim, M.M., Kuciauskas, D., Swain, S., Ablekim, T., Lynn, K.G. and Metzger, W.K. (2016) CdTe Solar Cells with Open-Circuit Voltage Breaking the 1 V Barrier. *Nature Energy*, **1**, Article No. 16015. https://doi.org/10.1038/nenergy.2016.15

[10] Jackson, P., Hariskos, D., Lotter, E., Paetel, S., Wuerz, R., Menner, R., Wischmann, W. and Powalla, M. (2011) New World Record Efficiency for Cu(In, Ga)Se_2 Thin-Film Solar Cells beyond 20%. *Progress in Photovoltaics*: *Research and Applications*, **19**, 894-897. https://doi.org/10.1002/pip.1078

[11] Wang, W., Winkler, M.T., Gunawan, O., Gokmen, T., Todorov, T.K., Zhu, Y. and Mitzi, D.B. (2014) Device Characteristics of CZTSSe Thin-Film Solar Cells with 12.6% Efficiency. *Advanced Energy Materials*, **4**, Article ID: 1301465. https://doi.org/10.1002/aenm.201301465

[12] Zimmermann, E., Pfadler, T., Kalb, J., Dorman, J.A., Sommer, D., Hahn, G., Weickert, J. and Schmidt-Mende, L. (2015) Toward High-Efficiency Solution-Processed Planar Heterojunction Sb_2S_3 Solar Cells. *Advanced Science*, **2**, Article ID: 1500059. https://doi.org/10.1002/advs.201500059

[13] Wen, X., Chen, C., Lu, S., Li, K., Kondrotas, R., Zhao, Y., Chen, W., Gao, L., Wang, C., Zhang, J., Niu, G. and Tang, J. (2018) Vapor Transport Deposition of Antimony Selenide Thin Film Solar Cells with 7.6% Efficiency. *Nature Communications*, **9**, Article No. 2179. https://doi.org/10.1038/s41467-018-04634-6

[14] Ghosh, C. and Varma, B.P. (1979) Optical Properties of Amorphous and Crystalline Sb_2S_3 Thin Films. *Thin Solid Films*, **60**, 61-65. https://doi.org/10.1016/0040-6090(79)90347-X

[15] Versavel, M.Y. and Haber, J.A. (2007) Structural and Optical Properties of Amorphous and Crystalline Antimony Sulfide Thin-Films. *Thin Solid Films*, 515, 7171-7176. https://doi.org/10.1016/j.tsf.2007.03.043

[16] Boix, P.P., Lee, Y.H., Fabregat-Santiago, F., Im, S.H., Mora-Sero, I., Bisquert, J. and Seok, S.I. (2012) From Flat to Nanostructured Photovoltaics: Balance between Thickness of the Absorber and Charge Screening in Sensitized Solar Cells. *ACS Nano*, **6**, 873-880. https://doi.org/10.1021/nn204382k

[17] Lee, Y.H., Heo, J.H., Im, S.H., Kim, H.J., Lim, C.S., Ahn T.K. and Seok, S.I. (2013) Improvement of Nonlinear Response for the Power Conversion Efficiency with Light Intensities in Cobalt Complex Electrolyte System. *Chemical Physics Letters*, **573**, 63-69. https://doi.org/10.1016/j.cplett.2013.04.047

[18] Shuai, X. and Shen, W. (2012) A Facile Chemical Conversion Synthesis of Sb_2S_3 Nanotubes and the Visible Light-Driven Photocatalytic Activities. *Nanoscale Research Letters*, **7**, Article No. 199. https://doi.org/10.1186/1556-276X-7-199

[19] Ibuke, S. and Yochimatsu, S. (1955) Photoconductivity of Stibnite (Sb_2S_3). *Journal of the Physical Society of Japan*, **10**, 549-554. https://doi.org/10.1143/JPSJ.10.549

[20] Li, K., Huang, F. and Lin, X. (2008) Pristine Narrow-Bandgap Sb2S3 as a High-Efficiency Visible-Light Responsive Photocatalyst. *Scripta Materialia*, **58**, 834-837. https://doi.org/10.1016/j.scriptamat.2007.12.033

[21] Arivuoli, D., Gnanam, F. and Ramasamy, P. (1988) Growth and Microhardness Studies of Chalcogneides of Arsenic, Antimony and Bismuth. *Journal of Materials Science Letters*, **7**, 711-713. https://doi.org/10.1007/BF00722076

[22] Savadogo, O. and Mandal, K. (1992) Studies on New Chemically Deposited Photoconducting Antimony Trisulphide Thin Films. *Solar Energy Materials and Solar Cells*, **26**, 117-136. https://doi.org/10.1016/0927-0248(92)90131-8

[23] Han, Q., Chen, L., Wang, M., Yang, X., Lu, L. and Wang, X. (2010) Low-Temperature Synthesis of Uniform Sb_2S_3 Nanorods and Its Visible-Light-Driven Photocatalytic Activities. *Materials Science and Engineering*: *B*, **166**, 118-121. https://doi.org/10.1016/j.mseb.2009.10.010

[24] Sun, M., Li, D.Z., Li, W.J., Chen, Y.B., Chen, Z.X., He, Y.H. and Fu, X.Z. (2008) A New Photocatalyst, Sb_2S_3, for Degradation of Methyl Orange under Visible Light Irradiation. *The Journal of Physical Chemistry C*, **112**, 18076-18081. https://doi.org/10.1021/jp806496d

[25] Cao, X., Gu, L., Zhuge, L., Gao, W., Wang, W. and Wu, S. (2006) Template-Free Preparation of Hollow Sb2S3 Microspheres as Supports for Ag Nanoparticles and Photocatalytic Properties of the Constructed Metal—Semiconductor Nanostructures. *Advanced Functional Materials*, **16**, 896-902. https://doi.org/10.1002/adfm.200500422

[26] Zawawi, I., Moez, A., Terra, F. and Mounir, M. (1998) Substrate Temperature Effect on the Optical and Electrical Properties of Antimony Trisulfide Thin Films. *Thin Solid Films*, **324**, 300-304. https://doi.org/10.1016/S0040-6090(98)00350-2

[27] Mathew, N., Oommen, R., Rajalakshmi, U. and Sanjeeviraja, C. (2011) Investigations of the Se Doped Sb_2S_3 Thin Films. *Chalcogenide Letters*, **8**, 441-446.

[28] Messina, S., Nair, M. and Nair, P. (2007) Antimony Sulfide Thin Films in Chemically Deposited Thin Film Photovoltaic Cells. *Thin Solid Films*, **515**, 5777-5782. https://doi.org/10.1016/j.tsf.2006.12.155

[29] Lazcano, Y., Nair, M. and Nair, P. (2005) Photovoltaic p-i-n Structure of Sb_2S_3 and $CuSbS_2$ Absorber Films Obtained via Chemical Bath Deposition. *Journal of the Electrochemical Society*, **152**, 635-638. https://doi.org/10.1149/1.1945387

[30] Mane, R.S. and Lokhande, C.D. (2003) Photoelectrochemical Cells Based on Nanocrystalline Sb_2S_3 Thin Films. *Materials Chemistry and Physics*, **78**, 385-392. https://doi.org/10.1016/S0254-0584(02)00155-4

[31] Savadogo, O. (1998) Chemically and Electrochemically Deposited Thin Films for Solar Energy Materials. *Solar Energy Materials and Solar Cells*, **52**, 361-388. https://doi.org/10.1016/S0927-0248(97)00247-X

[32] Perales, E., Lifante, G., Rueda, F. and Hares, C. (2007) Optical and Structural Properties in the Amorphous to Polycrystalline Transition in Sb_2S_3 Thin Films. *Journal of Physics D: Applied Physics*, **40**, 2440-2444. https://doi.org/10.1088/0022-3727/40/8/005

[33] Perales, E., Rueda, F., Lamela, J. and Heras, C. (2008) Optical and Structural Properties of Sb_2S_3/MgF_2 Multilayers for Laser Applications. *Journal of Physics D: Applied Physics*, **41**, Article ID: 045403. https://doi.org/10.1088/0022-3727/41/4/045403

[34] Arun, P., Vedeshwar, A. and Mehra, N. (1997) Laser-Induced Crystallization in Sb_2S_3 Films. *Materials Research Bulletin*, **32**, 907-913. https://doi.org/10.1016/S0025-5408(97)00064-0

[35] Herzog, V.Z., Bassell, S.L.H., Nesbitt, H.W. and Pratt, A.R. (2006) High Resolution XPS Study of the Large-Band-Gap Semiconductor Stibnite (Sb_2S_3): Structural Contributions and Surface Reconstruction. *Surface Science*, **600**, 348-356. https://doi.org/10.1016/j.susc.2005.10.034

[36] Garcia, R.G.A., Avendaño, C.A.M., Pal, M., Delgado, F.P. and Mathews, N.R. (2016) Antimony Sulfide (Sb_2S_3) Thin Films by Pulse Electrodeposition: Effect of Thermal Treatment on Structural, Optical and Electrical Properties. *Materials Science in Semiconductor Processing*, **44**, 91-100. https://doi.org/10.1016/j.mssp.2015.12.018

[37] Grigas, J., Talik, E. and Lazauska, V. (2002) X-Ray Photoelectron Spectroscopy of Sb_2S_3 Crystals. *Phase Transitions*, **75**, 323-337. https://doi.org/10.1080/01411590290020448